optica

Entanglement demonstration on board a nano-satellite

Aitor Villar,[1,*] Alexander Lohrmann,[1] Xueliang Bai,[1] Tom Vergoossen,[1] Robert Bedington,[1] Chithrabhanu Perumangatt,[1] Huai Ying Lim,[1] Tanvirul Islam,[1] Ayesha Reezwana,[1] Zhongkan Tang,[1] Rakhitha Chandrasekara,[1] Subash Sachidananda,[1] Kadir Durak,[1,2] Christoph F. Wildfeuer,[3] Douglas Griffin,[4] Daniel K. L. Oi,[5] and Alexander Ling[1,6]

[1]Centre for Quantum Technologies, National University of Singapore, 3 Science Drive 2, S117543 Singapore, Singapore
[2]Current address: Department of Electrical and Electronics Engineering, Özyeğin University, 34794 Istanbul, Turkey
[3]FHNW University of Applied Sciences and Arts Northwestern Switzerland, School of Engineering, Klosterzelgstrasse 2, CH-5210 Windisch, Switzerland
[4]University of New South Wales Canberra, School of Engineering and Information Technology, Canberra NSW, Australia
[5]SUPA Department of Physics, University of Strathclyde, John Anderson Building, 107 Rottenrow East, G4 0NG Glasgow, UK
[6]Physics Department, National University of Singapore, 2 Science Drive 3, S117542 Singapore, Singapore
*Corresponding author: aitor.villar@u.nus.edu

Received 6 January 2020; revised 30 April 2020; accepted 25 May 2020 (Doc. ID 387306); published 25 June 2020

Global quantum networks for secure communication can be realized using large fleets of satellites distributing entangled photon pairs between ground-based nodes. Because the cost of a satellite depends on its size, the smallest satellites will be most cost-effective. This Letter describes a miniaturized, polarization entangled, photon-pair source operating on board a nano-satellite. The source violates Bell's inequality with a Clauser–Horne–Shimony–Holt parameter of 2.60 ± 0.06. This source can be combined with optical link technologies to enable future quantum communication nano-satellite missions.

https://doi.org/10.1364/OPTICA.387306

Quantum entanglement describes non-local correlation between multiple bodies such that their wavefunction is irreducible to a product of individual wavefunctions. Entanglement correlations [1–5] have emerged as an essential resource in quantum technologies, and entanglement is used in various fields such as computation [6], sensing [7], and communication [8].

Near-term applications include quantum key distribution (QKD), where entanglement can be used to quantify knowledge gained by an adversary [8] and to enable device-independent encryption [9]. Beyond the immediate advantages for near-term technologies (such as QKD), efforts and resources are being directed towards the development of a quantum internet [10,11]. Such a network is envisioned to feature quantum nodes that are capable of producing, detecting, or verifying quantum entanglement. A global quantum network can be more readily realized using space-based nodes [11–13].

The first steps towards space-based nodes have been taken [14–19], and major milestones that demonstrate space-based quantum communication primitives have been achieved by the Micius satellite [17,18,20]. These pioneering space experiments used sizable satellite platforms with significant resources; the satellite mass in the space-based communication experiments have ranged between 50 kg [19] to 600 kg [18]. One opportunity for accelerating progress within the field is to utilize smaller, standardized spacecraft to enable cost-effective quantum nodes in space [21,22]. The de-facto standard spacecraft in the nano-satellite class is the CubeSat, where the most basic platform is a 10 cm cube (1U), and a growing family of proportionally larger (2U, 3U, 6U, 12U) spacecraft are also defined.

Previous work reported that photon pairs created by spontaneous parametric downconversion (SPDC) could be generated on board CubeSats [15]. This Letter reports on the essential next step: the generation and detection of polarization entangled photon pairs on board a CubeSat in low-Earth orbit (LEO). This demonstration marks a milestone towards realizing space-to-ground entanglement distribution from a CubeSat [23].

The in-orbit experiment occupies approximately 2U of volume in the 3U CubeSat, SpooQy-1 (Fig. 1, designed and built at the Centre for Quantum Technologies, National University of Singapore). The remaining 1U houses the spacecraft avionics. The experiment is composed of a source of entangled photon pairs coupled to a detector module [see Fig. 2(a)] all controlled by an integrated electronics subsystem. A micro-controller on the experiment interfaces to the satellite's on-board computer to receive commands and to return science data to ground control.

The polarization entangled photon-pair source is based on collinear, non-degenerate type-I SPDC with critically phase-matched non-linear crystals. The source design [Fig. 2(b)] uses a *parallel-crystal* configuration [24,25]. The beam overlap found in this design provides the source with better alignment stability in contrast to other two-crystal designs [26].

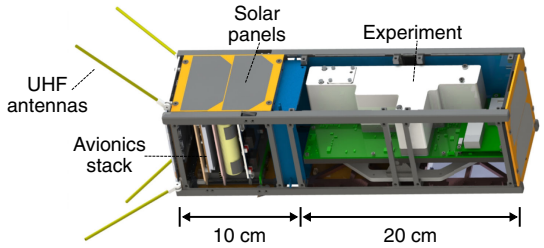

Fig. 1. Systems within the SpooQy-1 satellite (some solar panels not shown for clarity). Fully assembled, the CubeSat mass is 2.6 kg. The experiment has a volume of 206 mm × 85 mm × 49 mm, a mass of 0.9 kg, and its peak power consumption is 2.5 W.

A collimated laser diode (central wavelength $\lambda = 405$ nm, spectral linewidth $\Delta\nu = 160$ MHz) with a beam full-width half-maximum of 800 µm × 400 µm is used as a continuous-wave pump for the SPDC process. The pump produces horizontally polarized photon pairs in two β-barium borate (BBO-1 and BBO-2) crystals (cut angle, 28.8°; length, 6 mm). Between the two BBO crystals, an achromatic half-wave plate (HWP) induces a 90° rotation in the polarization of the SPDC photons from BBO-1, while the pump polarization remains unaffected.

The photon-pair source produces the state $|\phi\rangle = \frac{1}{\sqrt{2}}(|H_s\, H_i\rangle + e^{i\Delta\varphi}|V_s\, V_i\rangle)$, where s (i) denotes the signal (idler) photon wavelength, and $\Delta\varphi$ is the relative phase difference between photon pairs born in BBO-1 and BBO-2. Excess pump light is removed by a dichroic mirror to a detector that tracks power and pointing. An a-cut yttrium orthovanadate (YVO_4) crystal compensates for the birefringent dispersion of the SPDC photons (related to $\Delta\varphi$ [24]). The tilt angle of BBO-1 is adjusted such that the final phase difference $\Delta\varphi$ becomes π, generating the maximally entangled Bell state $|\Phi^-\rangle$.

The relative angle of the pump beam and the optical axis of the BBO crystals must be kept within 100 µrad in order to control the phase of the generated photon pairs (see Fig. S1 in Supplement 1). This can be achieved without active alignment using titanium flexure stages. To reduce misalignments resulting from a mismatch in the thermal expansion of different materials, the rest of the optical bench is also made of titanium.

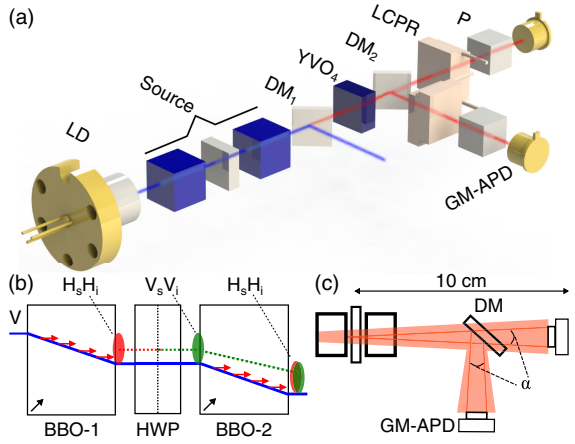

Fig. 2. (a) Essential optics in the experiment. LD, laser diode; DM, dichroic mirror; YVO_4, yttrium orthovanadate; LCPR, liquid-crystal polarisation rotator; P, polarizer; GM-APD, Geiger-mode avalanche-photodiode. (b) Entangled photon-pair source concept. This design facilitates either of the $|\Phi^{\pm}\rangle$ Bell states. (c) Collection condition of the SPDC photons (opening angle, α, 0.3°) detected by GM-APDs.

The SPDC photon pairs are separated by a dichroic mirror, and signal and idler photons have their polarization state analyzed separately. Each polarization analyzer is composed of a liquid-crystal polarization rotator (LCPR) followed by a polarizer [27]. Photon detection is performed using un-cooled, passively quenched, Geiger-mode avalanche photodiodes (GM-APDs, with detection efficiencies of 45% at 800 nm) with active areas of 500 µm located 10 cm away from the center of the source. Detection events are identified as correlations if they occur within a time window of 4.84 ± 0.06 ns.

To simplify the optical assembly, collection optics were not used. This collection condition, described in Fig. 2(c), restricts the light detection to SPDC photons with an opening angle, α, of 0.3°. While this affects the brightness, it does not detract from the primary objective of demonstrating in-orbit entanglement.

During the course of operation in orbit, the satellite experiences varying levels of solar illumination causing the temperature of the experiment to fluctuate. This can be mitigated by running a 2.5 W heater (Fig. S2 in Supplement 1). The temperature variation affects the breakdown voltage of the GM-APDs. To ensure a constant detection efficiency, the bias voltage of the detectors is optimized by a window comparator technique that tracks changes in the output pulse height of the GM-APDs [28].

To investigate the polarization correlation of the photon pairs, one arm is analyzed with fixed polarization (either H, horizontal; V, vertical; D, diagonal; or A, anti-diagonal), while the other arm is swept through different polarization states. In principle, the LCPR devices can achieve almost 2π of phase shift, but, towards the end of the range, the performance of the devices lack precision. To improve performance reliability, the LCPR devices were restricted to a phase shift of approximately 150 deg.

The visibility (contrast) of the polarization correlation curves can be used to assess the quality of the entangled state. Additionally, it is possible to extract 16 data points from these correlation curves. Each curve can provide four data points that are separated by 45° (see Fig. 3). These data points are used to obtain a measure of entanglement known as the Clauser–Horne–Shimony–Holt (CHSH) [29] parameter, S.

After assembly of the satellite, the on-ground detected pair rate (combined for both polarization bases) is 1400 pairs/s at approximately 17 mW of pump power (≈ 590, 000 singles/s for signal and idler). The visibilities (corrected for accidentals) recorded in the two bases (H/V and D/A) were $V_H = 0.97 \pm 0.05$, $V_V = 0.97 \pm 0.06$, $V_D = 0.84 \pm 0.05$, and $V_A = 0.90 \pm 0.05$. From these curves, a CHSH parameter of 2.63 ± 0.07 was extracted [see Fig. 3(a)]. If used for quantum communication, this source would introduce an intrinsic quantum bit error ratio (QBER) of approximately $3.9 \pm 0.4\%$.

The satellite was deployed into orbit from the International Space station on 17th June 2019 (orbit inclination: 51.6°, 408 km altitude) and operations began on the same day. The temperature of the experiment fluctuated according to the diurnal cycle of the satellite's 90 min orbital period as expected. To bring the experiment within the range of operating temperature, the on-board heater was activated (see Fig. S2 in Supplement 1). The difference between the on-ground and in-orbit temperatures made it necessary to recalibrate the LCPR devices and to operate the experiment in orbit with a different pump current (see Fig. S3 in

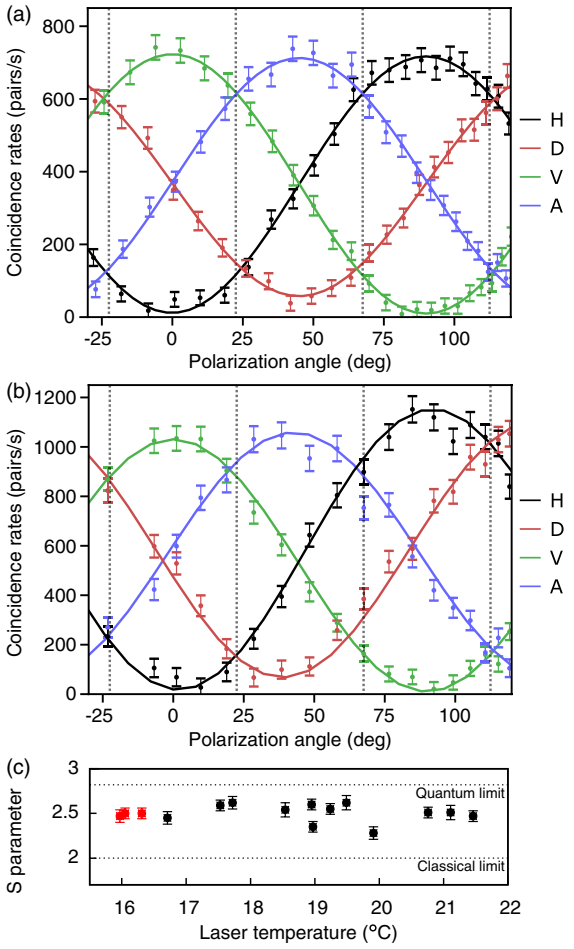

Fig. 3. (a) On-ground polarization correlation curves after the experiment was integrated into the satellite. Average visibility at 20°C (corrected for accidental coincidences) recorded in the two bases (H/V and D/A) were $V_{H/V} = 0.97 \pm 0.05$ and $V_{D/A} = 0.87 \pm 0.05$. The corresponding CHSH parameter was 2.63 ± 0.07. The dashed, vertical lines indicate the settings used to obtain the CHSH parameter. (b) Correlation curves measured in orbit on 16th July 2019. For clarity, only a subset of data points are shown. The average visibility (corrected for accidental coincidences) at 17.5°C was $V_{H/V} = 0.98 \pm 0.06$ and $V_{D/A} = 0.88 \pm 0.06$. The corresponding CHSH parameter of 2.60 ± 0.06. (c) In-orbit CHSH values at different temperatures obtained over two weeks of operation. The red-colored data points were taken after the satellite was under direct solar illumination for 100 h (see Fig. S2 in Supplement 1).

Supplement 1), which can yield a different laser mode, leading to slightly different brightness levels.

The typical in-orbit detected pair rate (combined for both polarization bases) was 2200 pairs/s ($\approx 700,000$ singles/s for signal and idler). The highest recorded visibilities were: $V_H = 0.98 \pm 0.05$, $V_V = 0.97 \pm 0.06$, $V_D = 0.88 \pm 0.06$, and $V_A = 0.88 \pm 0.06$. These visibilities yielded a CHSH parameter of $V_H = 2.60 \pm 0.06$ [Fig. 3(b)]. This value is a slight underestimate of the actual CHSH parameter because the LCPR settings for the diagonal and anti-diagonal polarization states had a systematic error. This can be seen from Fig. 3(b), where the extrema of the correlation curves in the diagonal/anti-diagonal settings do not occur exactly at the D/A (45°/135°) basis setting. Nevertheless, this causes only a slight degradation in the CHSH value compared to the on-ground baseline value.

Entangled photon-pair production was observed over a temperature range from 16°C to 21.5°C [Fig. 3(c)]. The experiment experienced relatively high temperatures when the satellite entered an orbital condition of continuous solar illumination (no data was collected during this period). Data collection resumed after exiting continuous illumination, and pre-illumination performance was observed (see red data points in Fig. 3(c)].

The operation of a polarization entangled photon-pair source on board a CubeSat in LEO has been reported. This shows that entanglement technology can be deployed with minimal resources in novel operating environments, providing valuable 'space heritage' for different components and assembling techniques.

The next generation of the experiment can achieve an improvement of two orders of magnitude in the photon-pair rate [25], and other SPDC configurations are under consideration to enable other performance improvements [30]. A follow-on mission is under development where, the goal is to share entanglement between a nano-satellite and a ground receiver [23]. To achieve this goal, it is necessary to equip a nano-satellite with an optical terminal that has a pointing capability of approximately 10 μrad [22]. While this additional infrastructure is demanding, solutions have been reported from the commercial sector [31].

The result from this in-orbit experiment paves the way for testing a variety of satellite-based quantum communication protocols using small standardized spacecraft such as CubeSats. These include placement of faint laser pulses in space to perform decoy-state QKD, or to install only quantum receivers on the CubeSats to enable an uplink configuration [32–34]. Beyond securing keys, two-way entanglement distribution can also enable secure time transfer [35] between satellites providing global navigation services. Such a capability can be demonstrated via inter-CubeSat quantum communication [36].

Miniaturized sources are not restricted to nano-satellites. They can also be useful for the development of quantum communication subsystems in larger spacecrafts. This Letter also shows that CubeSats are well-placed to perform in-orbit subsystem and device performance characterization to support the development of space missions with larger satellites.

As small standardized spacecraft are cost-effective, we anticipate an acceleration of space-based demonstration for quantum technologies in domains such as time keeping and sensing. The use of a standardized platform makes it easier to work towards a realistic miniaturization of the required technology and to scale up the number of space-based nodes with constellations of *quantum* nano-satellites to enable a global quantum internet.

Funding. National Research Foundation Singapore (NRF-CRP12-2013-02); UK Space Agency (NSTP3-FT-063, NSTP-QSTP).

Disclosures. The authors declare no conflicts of interest.

See Supplement 1 for supporting content.

REFERENCES

1. A. Einstein, B. Podolsky, and N. Rosen, Phys. Rev. **47**, 777 (1935).
2. E. Schrödinger, Sci. Nat. **23**, 844 (1935).
3. J. S. Bell, Physics **1**, 195 (1964).
4. S. J. Freedman and J. F. Clauser, Phys. Rev. Lett. **28**, 938 (1972).
5. A. Aspect, P. Grangier, and G. Roger, Phys. Rev. Lett. **47**, 460 (1981).

6. D. Loss and D. P. DiVincenzo, Phys. Rev. A **57**, 120 (1998).
7. C. L. Degen, F. Reinhard, and P. Cappellaro, Rev. Mod. Phys. **89**, 035002 (2017).
8. A. K. Ekert, Phys. Rev. Lett. **67**, 661 (1991).
9. A. Acin, N. Brunner, N. Gisin, S. Massar, S. Pironio, and V. Scarani, Phys. Rev. Lett. **98**, 230501 (2007).
10. H. J. Kimble, Nature **453**, 1023 (2008).
11. S. Wehner, D. Elkouss, and R. Hanson, Science **362**, eaam9288 (2018).
12. T. Vergoossen, S. Loarte, R. Bedington, H. Kuiper, and A. Ling, Acta Astronaut. **173**, 164 (2020).
13. S. Khatri, A. J. Brady, R. A. Desporte, M. P. Bart, and J. P. Dowling, arXiv:1912.06678 (2019).
14. G. Vallone, D. Bacco, D. Dequal, S. Gaiarin, V. Luceri, G. Bianco, and P. Villoresi, Phys. Rev. Lett. **115**, 040502 (2015).
15. Z. Tang, R. Chandrasekara, Y. C. Tan, C. Cheng, L. Sha, G. C. Hiang, D. K. Oi, and A. Ling, Phys. Rev. Appl. **5**, 054022 (2016).
16. K. Günthner, I. Khan, D. Elser, B. Stiller, Ö. Bayraktar, C. R. Müller, K. Saucke, D. Tröndle, F. Heine, S. Seel, P. Greulich, H. Zech, B. Gütlich, S. Philipp-May, C. Marquardt, and G. Leuchs, Optica **4**, 611 (2017).
17. J. Yin, Y. Cao, Y.-H. Li, S.-K. Liao, L. Zhang, J.-G. Ren, W.-Q. Cai, W.-Y. Liu, B. Li, H. Dai, G.-B. Li, Q.-M. Lu, Y.-H. Gong, Y. Xu, S.-L. Li, F.-Z. Li, Y.-Y. Yin, Z.-Q. Jiang, M. Li, J.-J. Jia, G. Ren, D. He, Y.-L. Zhou, X.-X. Zhang, N. Wang, X. Chang, Z.-C. Zhu, N.-L. Liu, Y.-A. Chen, C.-Y. Lu, R. Shu, C.-Z. Peng, J.-Y. Wang, and J.-W. Pan, Science **356**, 1140 (2017).
18. S.-K. Liao, W.-Q. Cai, W.-Y. Liu, L. Zhang, Y. Li, J.-G. Ren, J. Yin, Q. Shen, Y. Cao, Z.-P. Li, F.-Z. Li, X.-W. Chen, L.-H. Sun, J.-J. Jia, J.-C. Wu, X.-J. Jiang, J.-F. Wang, Y.-M. Huang, Q. Wang, Y.-L. Zhou, L. Deng, T. Xi, L. Ma, T. Hu, Q. Zhang, Y.-A. Chen, N.-L. Liu, X.-B. Wang, Z.-C. Zhu, C.-Y. Lu, R. Shu, C.-Z. Peng, J.-Y. Wang, and J.-W. Pan, Nature **549**, 43 (2017).
19. H. Takenaka, A. Carrasco-Casado, M. Fujiwara, M. Kitamura, M. Sasaki, and M. Toyoshima, Nat. Photonics **11**, 502 (2017).
20. S.-K. Liao, W.-Q. Cai, J. Handsteiner, B. Liu, J. Yin, L. Zhang, D. Rauch, M. Fink, J.-G. Ren, W.-Y. Liu, Y. Li, Q. Shen, Y. Cao, F.-Z. Li, J.-F. Wang, Y.-M. Huang, L. Deng, T. Xi, L. Ma, T. Hu, L. Li, N.-L. Liu, F. Koidl, P. Wang, Y.-A. Chen, X.-B. Wang, M. Steindorfer, G. Kirchner, C.-Y. Lu, R. Shu, R. Ursin, T. Scheidl, C.-Z. Peng, J.-Y. Wang, A. Zeilinger, and J.-W. Pan, Phys. Rev. Lett. **120**, 030501 (2018).
21. W. Morong, A. Ling, and D. Oi, Opt. Photon. News **23**(10), 42 (2012).
22. D. K. Oi, A. Ling, G. Vallone, P. Villoresi, S. Greenland, E. Kerr, M. Macdonald, H. Weinfurter, H. Kuiper, E. Charbon, and R. Ursin, EPJ Quantum Technol. **4**, 6 (2017).
23. Centre for Quantum Technologies, "Singapore and UK collaborate on S18m project to develop quantum-secured communications networks," Centre for Quantum Technologies, 2018, https://www.quantumlah.org/about/highlight/2018-09-singapore-uk-quantum-communications-networks.
24. A. Villar, A. Lohrmann, and A. Ling, Opt. Express **26**, 12396 (2018).
25. A. Lohrmann, A. Villar, A. Stolk, and A. Ling, Appl. Phys. Lett. **113**, 171109 (2018).
26. P. Trojek and H. Weinfurter, Appl. Phys. Lett. **92**, 211103 (2008).
27. A. Lohrmann, C. Perumgatt, and A. Ling, Opt. Express **27**, 13765 (2019).
28. S. Sachidananda and A. Ling, arXiv:1111.2656 (2011).
29. J. F. Clauser, M. A. Horne, A. Shimony, and R. A. Holt, Phys. Rev. Lett. **23**, 880 (1969).
30. A. Lohrmann, C. Perumangatt, A. Villar, and A. Ling, Appl. Phys. Lett. **116**, 021101 (2020).
31. M. Storm, H. Cao, S. Litvinovitch, K. Puffenberger, M. Albert, J. Young, D. Pachowicz, and T. Deely, in *Big Data From Small Satellites 2, (AIAA/USU Conference on Small Satellites, SSC17-XI-09* (2017), p. 1–4.
32. T. Jennewein, C. Grant, E. Choi, C. Pugh, C. Holloway, J.-P. Bourgoin, H. Hakima, B. Higgins, and R. Zee, Proc. SPIE **9254**, 925402 (2014).
33. , The CSUG Team, E. Kerstel, A. Gardelein, M. Barthelemy, M. Fink, S. K. Joshi, and R. Ursin, EPJ Quantum Technol. **5**, 6 (2018).
34. R. Haber, D. Garbe, K. Schilling, and W. Rosenfeld, in *Advanced Technologies I, (AIAA/USU Conference on Small Satellites, SSC18-III-05* (2018), p. 1–8.
35. J. Lee, L. Shen, A. Ceré, J. Troupe, A. Lamas-Linares, and C. Kurtsiefer, Appl. Phys. Lett. **114**, 101102 (2019).
36. D. P. Naughton, R. Bedington, S. Barraclough, T. Islam, D. Griffin, B. Smith, J. Kurtz, A. S. Alenin, I. J. Vaughn, A. Ramana, I. Dimitrijevic, Z. S. Tang, C. Kurtsiefer, A. Ling, and R. Boyce, Opt. Eng. **58**, 016106 (2019).